The Meteoritical Society

Meteoritics & Planetary Science 44, Nr 7, 985–1000 (2009)
Abstract available online at http://meteoritics.org

The Carancas meteorite impact crater, Peru: Geologic surveying and modeling of crater formation and atmospheric passage

T. KENKMANN[1*], N. A. ARTEMIEVA[2], K. WÜNNEMANN[1], M. H. POELCHAU[1], D. ELBESHAUSEN[1], and H. NÚÑEZ DEL PRADO[3]

[1]Museum für Naturkunde— Mineralogie, Leibniz Institut an der Humboldt-Universität Berlin, Invalidenstrasse 43, D-10115 Berlin, Germany
[2]Institute of Geospheres Dynamics, Russian Academy of Sciences, Moscow, Russia
[3]Instituto Geológico Minero y Metalúrgico (INGEMMET), San Borja, Lima, Peru
[*]Corresponding author. E-mail: thomas.kenkmann@mfn-berlin.de

(Submitted 01 December 2008; revision accepted 21 May 2009)

Abstract—The recent Carancas meteorite impact event caused a worldwide sensation. An H4–5 chondrite struck the Earth south of Lake Titicaca in Peru on September 15, 2007, and formed a crater 14.2 m across. It is the smallest, youngest, and one of two eye-witnessed impact crater events on Earth. The impact violated the hitherto existing view that stony meteorites below a size of 100 m undergo major disruption and deceleration during their passage through the atmosphere and are not capable of producing craters. Fragmentation occurs if the strength of the meteoroid is less than the aerodynamic stresses that occur in flight. The small fragments that result from a breakup rain down at terminal velocity and are not capable of producing impact craters. The Carancas cratering event, however, demonstrates that meter-sized stony meteoroids indeed can survive the atmospheric passage under specific circumstances. We present results of a detailed geologic survey of the crater and its ejecta. To constrain the possible range of impact parameters we carried out numerical models of crater formation with the *iSALE* hydrocode in two and three dimensions. Depending on the strength properties of the target, the impact energies range between approximately 100–1000 MJ (0.024–0.24 t TNT). By modeling the atmospheric traverse we demonstrate that low cosmic velocities (12–14 kms^{-1}) and shallow entry angles (<20°) are prerequisites to keep aerodynamic stresses low (<10 MPa) and thus to prevent fragmentation of stony meteoroids with standard strength properties. This scenario results in a strong meteoroid deceleration, a deflection of the trajectory to a steeper impact angle (40–60°), and an impact velocity of 350–600 ms^{-1}, which is insufficient to produce a shock wave and significant shock effects in target minerals. Aerodynamic and crater modeling are consistent with field data and our microscopic inspection. However, these data are in conflict with trajectories inferred from the analysis of infrasound signals.

INTRODUCTION

The Earth undergoes a constant bombardment by near-Earth objects (NEOs). Small bodies are encountered more frequently than larger ones (Brown et al. 2002). The Earth's atmosphere acts as an effective protection shield for small NEOs (Morrison 2002). These meteoroids get disrupted into small fragments during their traverse through the atmosphere, decelerate to terminal velocity by atmospheric drag, and thus do not cause any damage on Earth. Disruption of meteoroids starts when aerodynamic stresses exceed the strength of the body (Ceplecha et al. 1993; Artemieva and Shuvalov 2001). A meteoroid's strength depends on its composition, structure, and mass. For instance, iron meteoroids are capable of resisting much higher aerodynamic stresses than stony meteoroids and therefore transfer three orders of magnitude more energy per unit area onto the Earth than stony meteoroids over the mass range of 10^3–10^7 kg (Bland and Artemieva 2006). The increase of strength with decreasing size is caused by a decrease in the number of flaws and fractures that control the bulk strength of the body (Weibull law 1951). All previously observed fireballs of chondritic bodies have shown severe fragmentation (Trigo-Rodríguez et al. 2006; Borovička and Spurný 2008). Disruption of meteoroids is documented in a number of witnessed falls and strewn fields, e.g., Neuschwanstein (Spurný et al. 2003) or Sikhote-Alin (Tsvetkov 1983). Meter- to decameter-sized crater pits that are frequent in strewn fields are always formed by iron

meteorites. Hence, the Carancas meteoroid fall is uncommon in several respects and appears to be incompatible with our present knowledge of the atmospheric entry and traverse of meteoroids through the atmosphere: (i) the stony meteoroid predominantly remained intact during traverse through the atmosphere, (ii) it did not form a meteorite strewn field, (iii) and was capable of producing a small impact crater.

This contribution presents a detailed geologic survey of the crater structure and provides a parameter study to better constrain the impact conditions for the Carancas event. It also includes a review of observations and interpretations of the Carancas event that have been published so far. We demonstrate that specific conditions exist under which even stony meteorites of common strength properties and a few meters in size are capable of surviving the atmospheric passage without fragmentation. These encounters change the probability assessment of small impact events.

The Carancas Meteoroid Fall on September 15, 2007—Observations

On September 15, 2007, at noon (11:45 h local time; 16:45 UTC) a bright fireball was observed in the sky from several places along the southern shore of Lake Titicaca in Bolivia and Peru (Tancredi et al. 2008a). Most observations were reported from the city of Desaguadero, which is situated at the Peruvian/Bolivian border about 12 km north of the point of impact. The meteorite hit the ground of the Puno region south of the village of Carancas, at W69.0441°/S16.6645°, altitude of 3826 m (Macedo and Macharé 2007). The fireball and its trajectory were witnessed by a number of people. These reports suggest an atmospheric passage from E to W (Tancredi et al. 2008a), or from NE to SW (Schultz et al. 2008). The report by Macedo and Macaré (2007), who described a passage towards NNE, is in conflict with the previous trajectories. A photograph of a smoke trail that was affected by upper-level winds was taken some 5–7 minutes after the fall. The meteoroid did not break apart and did not produce a strewn field. The meteorite impacted into unconsolidated soil and sand that was water-saturated at a depth of 1–1.5 m (Fig. 1). Residents of the community of Carancas situated ~3 km NNW of the point of impact heard a loud explosion, followed by the formation of a mushroom cloud composed of disseminated water droplets, dust, and fine-grained particles. The crater cavity immediately filled with water as the ground water table was breached. Ascending water bubbles were observed minutes after the impact (Tancredi et al. 2008a). They were most likely formed by the release of air that was trapped and compressed into the target in front of the impacting meteoroid. About 15 minutes after the impact, 1–2 m sized blocks of grassy uppermost soil slid down the steep western crater wall (Schultz et al. 2008). These slump blocks are shown in the geological map (Fig. 2a).

The Carancas Meteoroid Fall on September 15, 2007—Measurements and Interpretations

The entry of the Carancas meteoroid produced infrasound waves that were recorded by two infrasound arrays of the International Monitoring System for the enforcement of the Comprehensive Nuclear-Test-Ban Treaty (CTBT) 80 km northeast and 1,617 km southeast of the crater (Brown et al. 2008; Le Pichon et al. 2008). Azimuth and entry angle derived from the observed signal time sequences and back azimuths were estimated to be 110° and 50° from the horizontal (Le Pichon et al. 2008). Brown et al. (2008) derived an azimuth of 82° and an entry angle of 63°. While Le Pichon et al. (2008) expect an initial energy release during atmospheric entry in the range of 1–8 kt TNT equivalent (4,200–33,000 GJ), Brown et al. (2008) estimate 0.06–0.32 kt TNT equivalent (250–1,300 GJ). Both studies infer a rather low atmospheric entry speed of the meteoroid in the order of 12 kms^{-1} (Brown et al. 2008; Le Pichon et al. 2008).

The impact velocity was estimated in a number of recent studies and shows a remarkable range: 4–6 kms^{-1} (Harris et al. 2008), >3 kms^{-1} (Tancredi et al. 2008b), 3 kms^{-1} (Tancredi et al. 2008a), 2–4 kms^{-1} (Borovička and Spurný 2008), 1.5–4 kms^{-1} (Brown et al. 2008); >1.5 kms^{-1} (Le Pichon et al. 2008), and 0.2–0.3 kms^{-1} (Kenkmann et al. 2008a, 2008b).

Several attempts have been made to estimate the impact energy. Applying scaling laws of Housen and Holsapple (2007), Tancredi et al. (2008a) estimated an impact energy of 2 t TNT (8,360 MJ) and Tancredi et al. (2008b) estimated 3 t TNT (12,540 MJ). Based on yield scaling of explosions, Le Pichon et al. (2008) estimated an impact energy of 4.8 t TNT (20,060 MJ). In strong contrast Kenkmann et al. (2008b) derived only 62 MJ (0.015 t TNT), based on numerical modeling of crater formation and aerodynamic passage of the meteoroid through the atmosphere.

Attempts to estimate the shock pressure base on the recognition of shock features in target rocks. Cardona et al. (2008) describe 20–30 cm long shatter cones (it should be noted that it is impossible for shatter cones to form in unconsolidated loose soil [Baratoux and Melosh 2003], and clasts of consolidated rocks of 20 cm size embedded in the soil are not present at Carancas). Harris et al. (2008) found impactor fragments injected into strata suggesting a fully coupled collision of an intact meteoroid with the ground. They report finding grains with tentatively identifiable shock-induced microfabrics in both proximal and distal ejecta samples. They present photomicrographs with faint planar microfabrics in quartz and feldspar, which they interpreted as basal lamellae in quartz and planar deformation features in feldspar. The former suggests pressures >5–7 GPa (Stöffler and Langenhorst 1994), the latter shock pressures >10.5 GPa (Ostertag 1983). Cardona et al. (2008) observed arrays of fluid inclusions, which they interpret as decorated planar

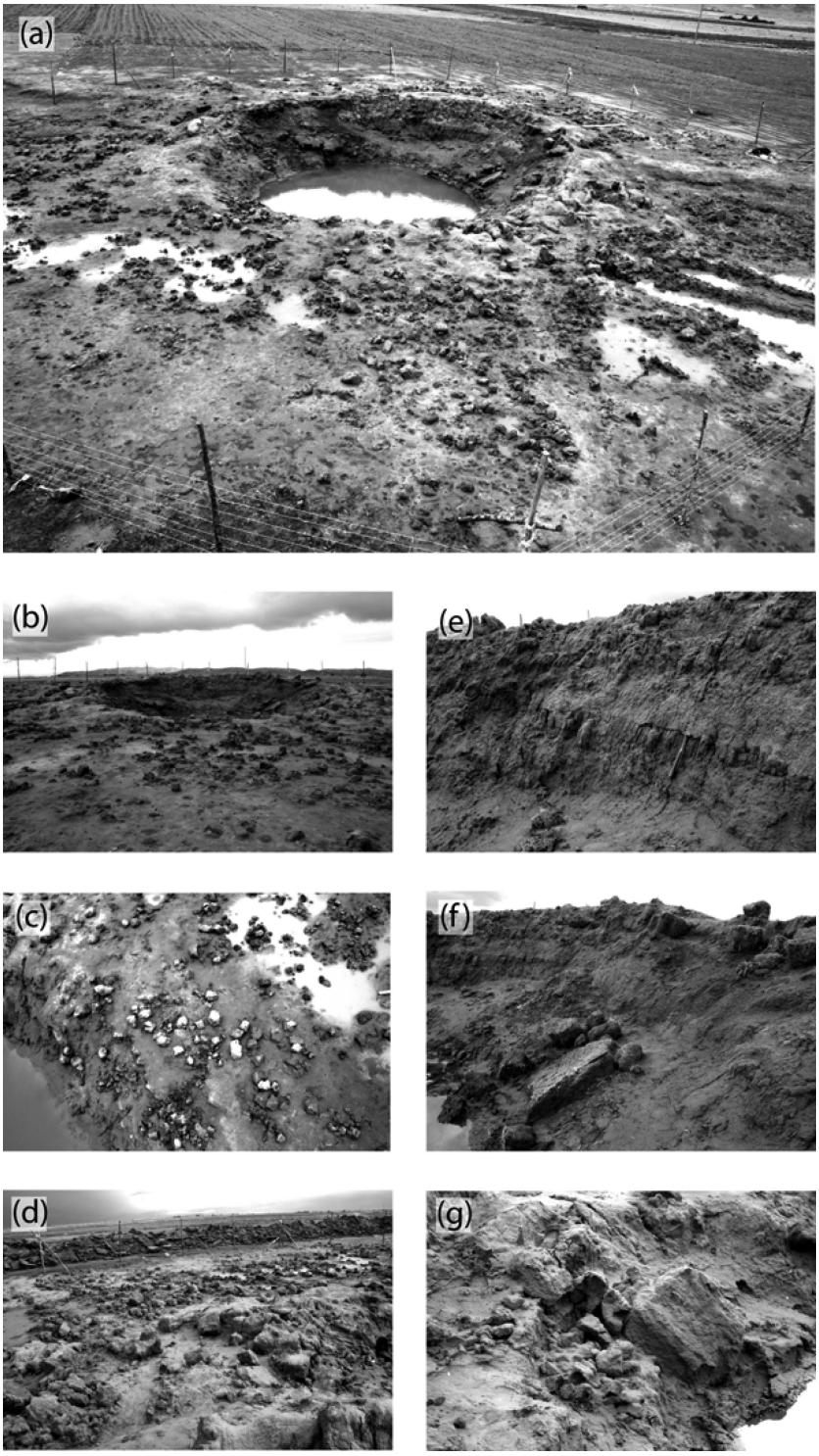

Fig. 1. Photographs of the Carancas meteorite impact crater taken 3½ months after the impact. a) Aerial photograph taken from E from a height of ~7 m. The crater is 14.2 m across and formed at the edge of a creek bank. The ~1 m slope between the terrace and creek bed trends NW-SE and divides the crater into two parts. b) The continuous ejecta blanket E of the crater is dominated by gravelly sand and extends about 4 m from the crater rim. c) Aerial photograph of the ejecta blanket SE of the crater, taken from a height of 6 m. Red sand fragments and dark soil blocks can easily be distinguished. A mosaic consisting of 94 of such aerial photographs was used as a basis for constructing the geological map in Fig. 2. d) Close-up of the ejecta blanket, looking from the eastern crater rim toward SE. e) Steep inner slope at the western side of the crater. The upper end of the hammer marks the suture between the autochthonous target and the overturned ejecta blanket. f) Slumped soil blocks indicating synthetic as well as antithetic block rotation. g) Sand blocks covering the inner slope of the eastern crater wall. Largest blocks are close to 1 m in size.

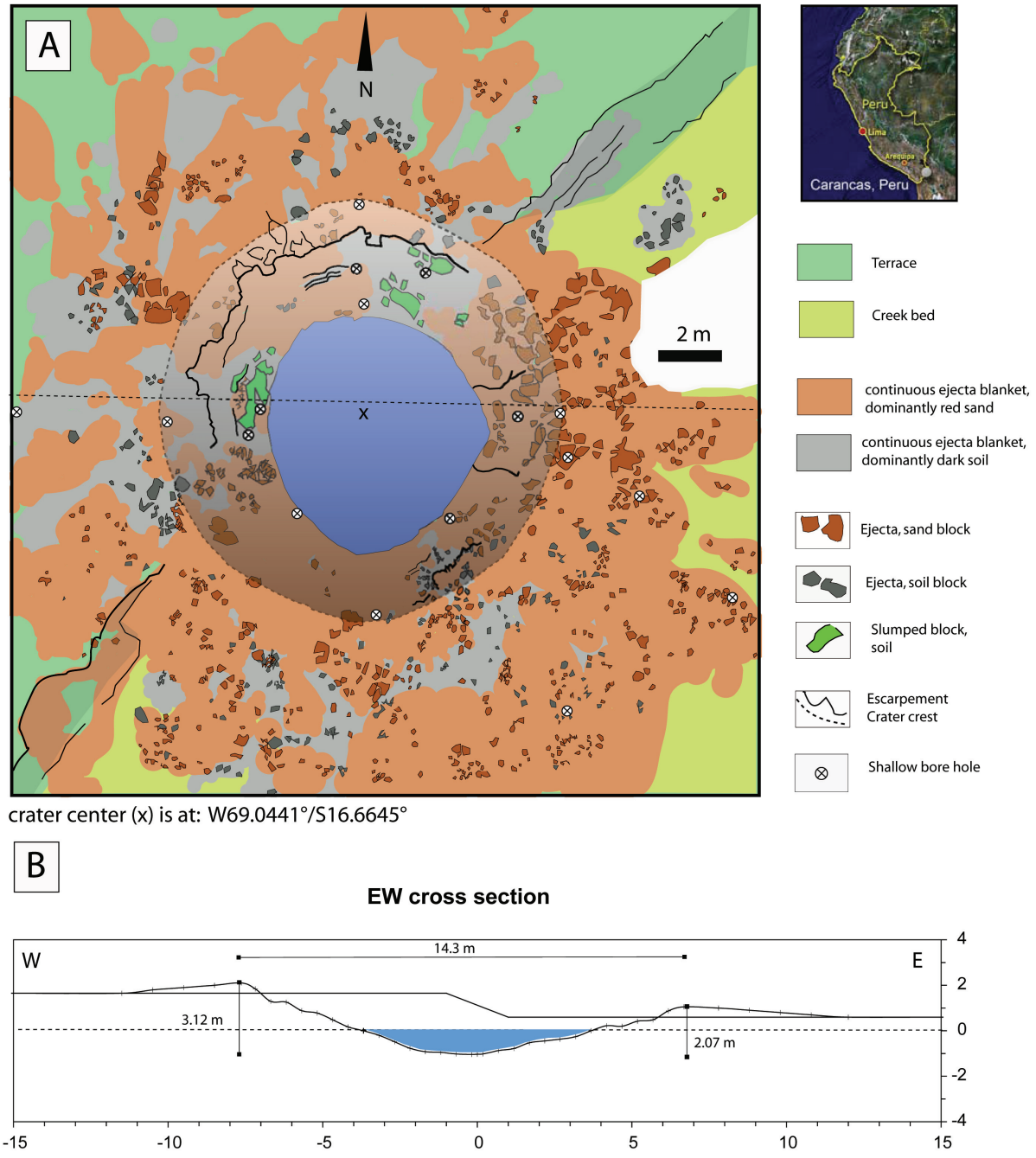

Fig. 2. A) Geological map of the Carancas meteorite impact crater, Peru. The stippled line delineates the crater crest. Two ejecta lithologies were distinguished based on aerial mapping: An ejecta blanket dominated by reddish sand and one dominated by dark soil. Blocks were separately mapped at sizes >0.2 m. Note that the crater pond is offset to the SE with respect to the crater center and has two corners in E and S direction. B) E-W cross section through the crater indicates the effect of the topography on crater formation. The depth/diameter ratio of the crater is 0.22 and 0.15, using the altitude difference from the terrace and creek bed to the crater center, respectively. We assume an average depth/diameter ratio of 0.18.

deformation features (PDF) in quartz. They inferred shock pressures in the range of 8–12 GPa. In search for possible shock features, we investigated samples from the crater wall, 18 shallow drill cores, and from the proximal and distal ejecta. We were unable to identify shock feature in any of their samples (see section Crater lithology and rock deformation). Miura (2007) assumed that the excavation process was followed by an explosion caused by the interaction of the hot meteoritic material with cold water and subsequent vaporization of water.

What makes Carancas unique is the fact that a stony meteoroid was capable of penetrating the atmosphere without

fragmentation. Schultz et al. (2008), Kenkmann et al. (2008a), and Borovička and Spurný (2008) provide three different explanations of how the Carancas stony meteoroid survived the atmospheric passage:

1. Based on experimental and theoretical models, Schultz et al. (2008) propose a scenario in which the meteoroid reshaped during atmospheric entry into a train of fragments. The fragments were trapped within the Mach cone that developed during hypervelocity flight through the atmosphere and could not spread as suggested in the "pancake model" (Chyba et al. 1993). In this arrangement, deceleration during atmospheric passage is minimized and the aerodynamic stresses are reduced for the trailing fragments but not for the leading fragment.
2. By modeling the atmospheric traverse Kenkmann et al. (2008a, 2008b) demonstrate that low cosmic velocity, very shallow entry angle, and low projectile mass are prerequisites for minimizing aerodynamic stresses and increasing the probability of a survival of stony meteoroids with a standard dynamic strength of a few MPa.
3. Borovička and Spurný (2008) explain the absence of fragmentation of the Carancas bolide by an anomalously high tensile strength of the meteoroid, which must have been in the order of 20–40 MPa. They argue that the stony meteorite was a monolithic body free of internal cracks and generally conclude that rock strength is not scale-dependent, which is in conflict to fundamental rock mechanics (e.g., Weibull 1951; Adey and Pusch 1999).

The Carancas Meteorite

Fragments of the projectile that produced the crater, the Carancas meteorite, were distributed within the crater and in the surrounding ejecta. Fine-grained grayish meteorite powder was widely dispersed along the crater walls (Tancredi et al. 2008a). Local residents and many others have recovered numerous pieces of the impactor from the sides of the crater and the surrounding area, which amount to several kilograms. From this it is expected that the majority of the meteorite is still sticking within the crater floor. The Carancas meteorite is classified as a H4–5 ordinary chondrite (Connolly et al. 2007). According to the Meteoritical Bulletin (Connolly et al. 2007) most of the collected specimens have a gray color and no fusion crust. Chondrules and metal are occasionally visible. Dark-colored shock veins are present within meteorites and are exposed at fragment surfaces. At least one specimen was found that was composed of two different lithologies, suggesting that the Carancas meteorite is a breccia (Connolly et al. 2007). The Carancas meteorite experienced extensive recrystallization of the matrix with few relict chondrules present. These chondrules range in size from ~170 μm to 1 mm. Olivine ($Fa_{18.4 \pm 0.5}$) and orthopyroxene ($Fs_{16.1 \pm 0.2}$) were observed with abundant Fe, Ni-metal and Fe-rich sulfide (Connolly et al. 2007). Collected meteorite fragments have a remanent magnetization of 0.205 Gauss. A significant magnetic anomaly within the crater caused by a large meteorite that stuck in the crater floor could not be found (Rosales et al. 2008).

Most of the collected specimens show one or two dark colored faces that are striated and appear polished. We interpret these features as shear planes that were formed during the impact itself. Microscopic analysis revealed that brittle comminution of the brecciated host rock produced a very fine-grained groundmass that decorates these planes (Fig. 5a). Additional shock overprinting by the impact and localized melting by friction could not be observed on these polished surfaces.

FIELD DATA

Crater Morphology and Ejecta

To map the meteorite crater (Figs. 1a–b) in detail we surveyed the structure and systematically imaged the crater from an altitude of 6 m. For this purpose a camera system mounted onto a telescope rod was constructed that enabled us to take scaled photographs (Fig. 1c). A mosaic of 94 images covers the crater and its proximal ejecta blanket and provides the basis for mapping. Resolution of the geological map reaches down to block sizes of 0.2–0.3 m.

The Carancas impact crater is roughly circular in shape and has an average diameter of 14.2 ± 0.23 m, measured from rim crest to rim crest in 10° radial steps (Figs. 1 and 2). Data were taken 3.5 months after the event and give slightly larger values than measurements carried out shortly after the impact event (13.3–13.8 m, Macedo and Macharé 2007; 13.5 m; Núñez del Prado et a. 2008; Tancredi et al. 2008). These differences may indicate erosion and degradation of the crater rim. The crater formed at the edge of a ~1 m high creek bank. The creek bed is a periodic watercourse that was dry during the impact but contained subsurface water. The embankment influenced the crater morphology: (i) The crater cavity has higher and steeper slopes at the terrace (Figs. 1e, 2b, 3a). (ii) The steep slopes induced slumping of meter-sized soil blocks in the north and west (Figs. 1f, 2a). (iii) The center of the small crater pond is offset towards the creek bed (SE) with respect to the crater center (Fig. 2a). (iv) The crater rim on the terrace is higher than average, although scattering is large and slumping strongly modifies the height of the rim (Fig. 3b).

The average height of the crater rim is 54 cm above the target level. Depth/diameter ratios obtained from measured profiles through the crater (N-S and E-W cross sections) are 0.18–0.2 when averaging altitude differences (Fig. 2b). Drainage of loose sand into the crater cavity may have decreased the depth of the pond, which had a depth of 1.1 m at the time of surveying. The crater volume calculated from parabolas fitted to these cross sections is about 160 m^3. To

account for the sediment infill we ignored the depth measurements in the crater center for the parabola fitting.

The ejecta blanket has a maximum thickness along the rim crest and can locally reach 0.8–1 m. Along the steep inner crater slope the surface of the original target is occasionally exposed (Fig. 1e) and shows an inverted stratigraphy of the proximal ejecta. A suture line separates the autochthonous target from the overturned flap. The exposure of this marker line indicates that the hinge fold of the overturned flap is lacking and suggests that its removal took place by slumping. The ejecta consists of blocks of dark soil and reddish sand that form a continuous blanket to about 4 m from the crater rim. The continuous ejecta blanket in the southeastern creek bed has a wider extent than on the higher terrace and is dominated by sand and sand blocks that locally have sizes of 0.5 m (Figs. 1a–d). Blocks of dark soil are lacking in the western part of the ejecta blanket. Excavated blocks originally had angular shapes. Rounding of blocks (Figs. 1a–d) is caused by rainfall and erosion. Sizes of ejected boulders and fragments were measured along four radial profiles (Fig. 4). While scattering is large, the average block mass m [kg] decreases with radial range r [m] and obeys a power law ($m = 24.6\ r^{-0.89}$) (Fig. 4a). Based on a simplified geometrical assumption we estimated the volume of the proximal ejecta blanket. We assumed a torus ring with a maximum height at the crater crest and a linear decrease with increasing radial range, which yielded a volume of the proximal ejecta blanket of about 130 m^3. The distribution of the distal ejecta is strongly altered by soil cultivation around the crater. A maximum radial extent of 234 m from the crater was determined (Fig. 4b). Rosales et al. (2008) observed ejecta up to a distance of 248 m in the SW and up to 128 m in the NE. Schultz et al. (2008) reported that a 30° sector east of the crater was free of blocky ejecta.

Crater Lithology and Rock Deformation

Soils, loose sand, and consolidated sand/siltstones of the target were sampled at surface exposures of the crater and the ejecta as well as from eighteen shallow (1m) drillings. Their locations are given in the geological map (Fig. 2a). Bore holes were drilled to search for meteorite fragments and shocked material in the crater floor, and to obtain vertical profiles through the undisturbed and deformed target.

The target surface has a grass coverage and is composed of dark humus with abundant organic matter (O and A-horizons). The roots held blocks together of up to 50 cm in size during the excavation process. Beneath the topsoil horizon is a dark brown colored horizon in which the organic material mixes with inorganic products of weathering (B-horizon). This horizon shows variations in both thickness and composition. At the terrace it is 70–90 cm thick, in the creek bed 30–50 cm. Grain sizes in this horizon range from clay to sand and calcitic concretions occur occasionally. Loose reddish sand and silts occur beneath the soil that are not strongly affected by the soil forming processes. Grains are sub-rounded and grain size sorting is poor, with a clayey component present. The loose sands can contain lumps of unweathered Puno-Group sand- and siltstone beds underneath. Grains are dominantly composed of quartz, feldspar, amphibole, opaque phases, and polymineralic rock fragments of igneous provenance. Puno-Group sand/siltstones are composed of the same constituents as the overlying loose sand, but they are cemented by a calcite matrix (Figs. 5b–c). A few grains display transgranular fractures (Fig. 5c), which may be linked to the impact event. Shock features in quartz or feldspar could not be identified (Figs. 5d–e) and even the fracture densities in the constituents are not particularly high. The microscopic examination suggests that stresses were locally sufficient for tensile fracturing and shear fracturing.

CRATER FORMATION

Scaling Laws for Crater Formation

The observed crater dimensions raise the question of how big the meteorite was that made the crater. Since we do not know the impact velocity, it is impossible to deduce the size of the impactor only from crater dimensions. However, shape and size of the crater provide important constraints on the impact energy. So-called scaling-laws (e.g., Holsapple 1993) relate the kinetic energy of the projectile with the resulting crater dimensions depending on the properties of the target material (such as density ρ, cohesive strength Y, friction f, porosity ϕ) and gravity g (Holsapple and Housen 2007):

$$\frac{R}{a} = K_1 \left(\frac{ga}{U^2} \left(\frac{\rho}{\delta} \right)^{\frac{2\nu}{\mu}} + \left(\frac{Y}{\rho U^2} \right)^{\frac{2+\mu}{2}} \left(\frac{\rho}{\delta} \right)^{\frac{\nu(2+\mu)}{\mu}} \right)^{-\frac{\mu}{2+\mu}} \quad (1)$$

where R is the crater radius, and a, δ, U are radius, density and velocity (considering vertical impacts only) of the projectile, respectively. Note that crater radius refers to the size of the so-called transient crater that approximately corresponds to the size of the crater before slumping along crater walls or other gravity driven modifications occur. The scaling coefficients K_1, μ, and ν depend on material properties such as friction and/or porosity. In fact, these parameters can be only determined by laboratory (Schmidt and Housen 1987) or numerical experiments (e.g., O'Keefe and Ahrens 1993; Wünnemann et al. 2006), and are not well known for a large number of materials. The Carancas crater was formed in a material that is probably best approximated by wet sand. However, scaling parameters were determined only for dry sand ($K_1 = 1.03$, $\mu = 0.41$, $\nu = 0.4$) and water-saturated sand ($K_1 = 0.93$, $\mu = 0.55$, $\nu = 0.4$) (Holsapple and Housen 2007). With these parameters and an estimated transient crater

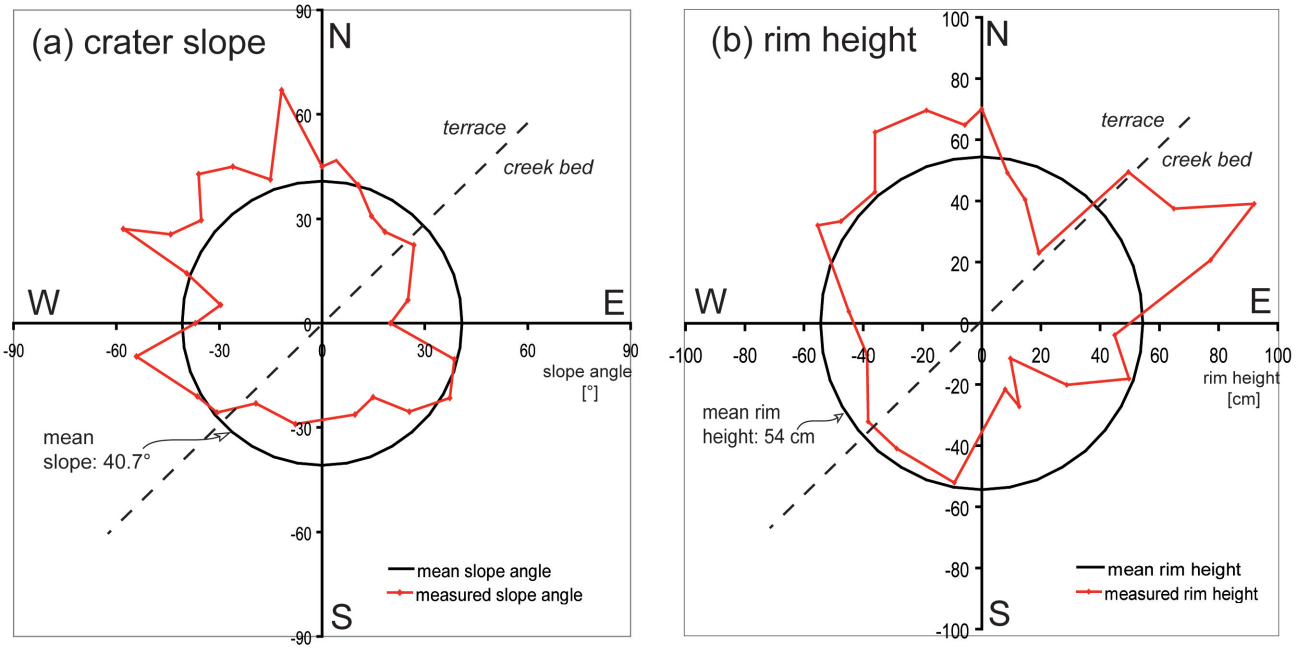

Fig. 3. a) Polar diagram of the crater slope at the target level. The slope of the inner crater wall is much steeper in the NW sector along the terrace than in the SE sector. While 40.7° represents the average inclination at the target level (black circle), the slope locally gets steeper than 60° at the terrace and decreases to 20° where the crater carved into the creek bed. b) Polar diagram of the rim height. The average thickness of the ejecta is 54 cm (black circle) at the rim crest. While an unusually thick overturned flap exists in the NE, the SE contains a very thin blanket.

diameter of 10 m, measured at the pre-impact surface level, the crater was formed with an impact energy of 83–233 MJ (water saturated sand, a = 1.0–0.18 m, δ = 3300 kgm^{-3}, Y = 1000 Pa, ρ = 2000 kgm^{-3}) or 134–1300 MJ (dry sand, a = 1.18–0.35 m, δ = 3300 kgm^{-3}, Y = 1000 Pa, ρ = 1500 kgm^{-3}) according to Equation 1, assuming an impact velocity of U = 0.1–2 kms^{-1}. Apparently, target properties such as friction and cohesion control the amount of energy required to produce a crater of the given size. Crater size is not directly proportional to the kinetic energy of the impactor (μ = 0.55 < 2/3 [energy scaling] in Equation 1). Thus, the impact energy necessary to form a cavity of the size of the Carancas crater is higher for high-velocity impacts and small projectile sizes than for low-velocity impacts and large projectiles. In conclusion, scaling laws do not provide very accurate estimates of the impact energy. However, in a range of reasonable estimates of the target properties the impact energy cannot have been much higher than 1300 MJ (0.3 t TNT equivalent) (U = 2 kms^{-1}) and even if we consider a velocity U = 6 kms^{-1} the impact energy is only 3000 MJ (0.7 t TNT equivalent), in stark contrast to Tancredi et al. (2008a,b), Le Pichon et al. 2008) and others.

Numerical Modeling of Crater Formation

To better constrain the range of plausible impact velocities, sizes, and energies of the impactor we carried out numerical models of crater formation with the *iSALE* hydrocode (for more details about the code see e.g., Wünnemann et al. 2006; Elbeshausen et al. 2009). In order to approximate the estimated density of wet soil for the target (~2 gcm^{-3}) and the chondritic composition of the projectile (3.5 gcm^{-3}) we chose wet tuff and dunite, respectively, as closest analogues for which material models (equations-of-state) are available. We used the Tillotson equation-of-state (Tillotson 1962) for the target (wet tuff; Allen 1967) and ANEOS (Thompson and Lauson 1972) for the projectile (dunite; Benz et al. 1989). For reasons related to the atmospheric traverse of the projectile that we will discuss in the next section on aerodynamic modeling, we assume relatively low impact velocities of 350–600 ms^{-1}. This is also justified by the lack of shock features in the crater floor (see above). Therefore, compressibility of the material plays only a minor role in the impact process and a more accurate thermodynamic model of material behavior would not result in significant changes in the model results. A much more important variable that influences crater formation is the resistance of the target against plastic deformation, its cohesive strength Y and friction f. Wet and dry soils have very little cohesion; however, friction significantly depends on the water content. We carried out a suite of more than 50 simulations with a resolution of 20 cells per projectile radius for different impact energies (sizes and velocities) and adjusted the coefficient of friction f and cohesion Y over a range typical for wet soil (Rajarama and Erbach 1999) to match the observed crater dimension. Good agreement between numerical models

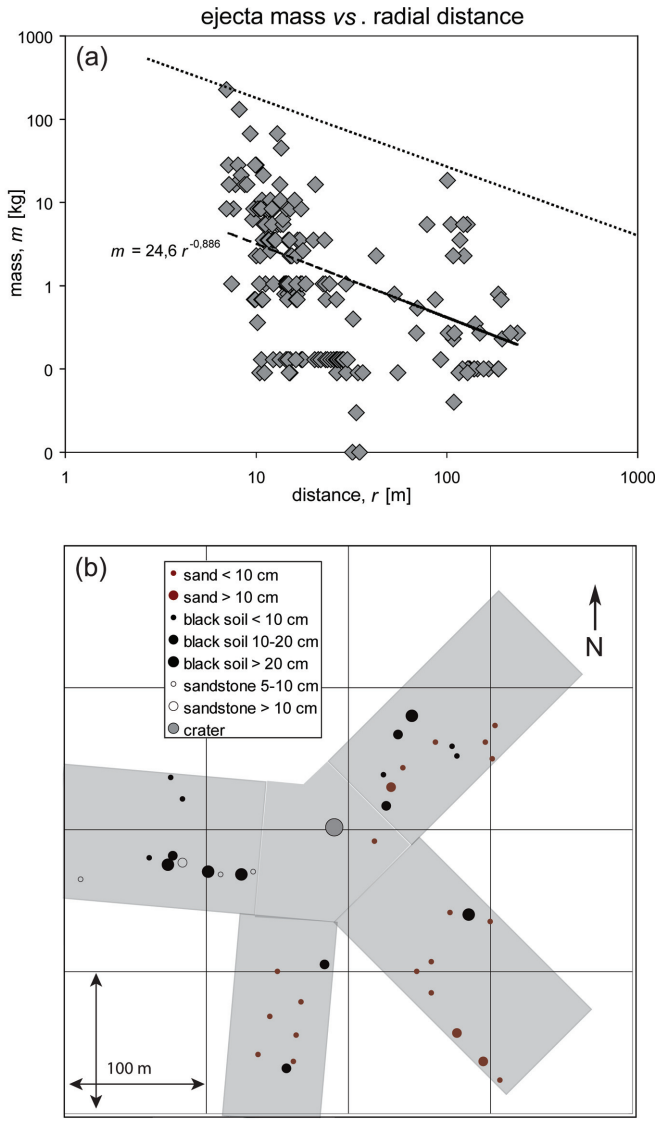

Fig. 4. a) Double logarithmic diagram of the mass of ejected fragments as a function of radial distance to the crater center. The mass of ejected blocks was calculated assuming sphere shapes and densities of 2 gcm^{-3} and 1.5 gcm^{-3} for sand and soil blocks, respectively. b) Distribution, size, and lithology of distal ejecta were investigated along four profiles (gray-shaded areas). The maximal radial extent was 234 m. Mapping of the distribution was strongly affected by soil cultivation.

and the observed crater morphometry (diameter, depth-diameter ratio) was achieved for a variety of model parameters: low-energy impacts require weak target properties (f = 0.35, Y = 1000 Pa) and high-energy impacts require stronger target properties (f = 0.7, Y = 1000 Pa). The two end-member cases for low-energy (E = 127 MJ, U = 350 ms^{-1}, a = 0.53 m) and high-energy (E = 1013 MJ, U = 600 ms^{-1}, a = 0.74 m) impacts are shown in Figs. 6a and 6b. The model agrees well with the observed crater dimensions when taking into account that the Carancas crater was enlarged by erosion. The depth of the Carancas crater is not well constrained due to the effect of slope failure and slumping from the sides. In our models the crater in the strong target is approximately 0.5 m deeper than the crater in the weak target. The diameter of the transient crater D_T differs between the two cases by almost 2 m (weak target: D_T = 9 m; strong target: D_T = 11 m) and is indicated by the dashed line in Figs. 6a and 6b. However, note the differences in crater morphology. The weaker target (f = 0.35, low energy impact, Fig. 6a) causes much more pronounced slumping and filling of the crater resulting in a more cone-shape crater morphology and smaller crater depth. In the high-energy case the stronger target (f = 0.7, Fig. 6b) impedes slumping and the final crater morphology is bowl-shaped, which is in better agreement with the observations.

Figures 6c and 6d and Table 1 show the pressure distribution in the target and in the relics of the projectile. For pressure calculations the mesh resolution was increased to 80 cells per projectile radius. The volume of material that experienced pressure larger than 2 GPa (the minimum shock pressure to produce shock features like shatter cones) is restricted to a volume of about 2.0–4.5 dm^3. The given pressure ranges in the target enable localized fracturing of quartz and feldspar grains but is two orders of magnitude too low to produce shock features in grains of the target. This is in agreement with our observations but contradicts data from Harris et al. (2008) and Cardona et al. (2008).

We carried out three-dimensional modeling where the projectile hits a 1 m slope of 30° inclination (Fig. 7) to account for the topography of the target and the oblique incidence of the projectile. By using the same parameters as in the 2D modeling (E = 127 MJ, U = 350 ms^{-1}, a = 0.53 m) we first considered a vertical impact onto the slope (Fig. 7a). We used the material properties for the weak target (f = 0.35, Y = 1000 Pa). Results of 3D modeling show a deviation from circularity in the transient crater shape, steep ejection angles towards the upper target level, and shallow ejection towards the lower target level. These results correlate with data obtained by geologic surveying of the crater, namely steep crater slopes and enhanced ejecta thickness along the rim of the terrace, and gentle crater slopes with a reduced ejecta thickness at the rim along the creek bed. In a second model, we changed the impact azimuth to 90° (impact towards W) (Brown et al. 2008; Le Pichon et al. 2008) and assumed an impact angle of 40° (see next paragraph). The final crater shape and distribution of ejecta is shown in plane view (Fig. 7b) and in perspective viewing from the upper target level towards SE and NE. The final crater is nearly circular (as the Carancas crater is), and the radial extent of the ejecta is reduced E of the crater (uprange sector) as it is the case for the Carancas crater (Fig. 2a).

MODELING OF THE AERODYNAMIC TRAVERSE

To reconstruct the passage of the Carancas meteoroid

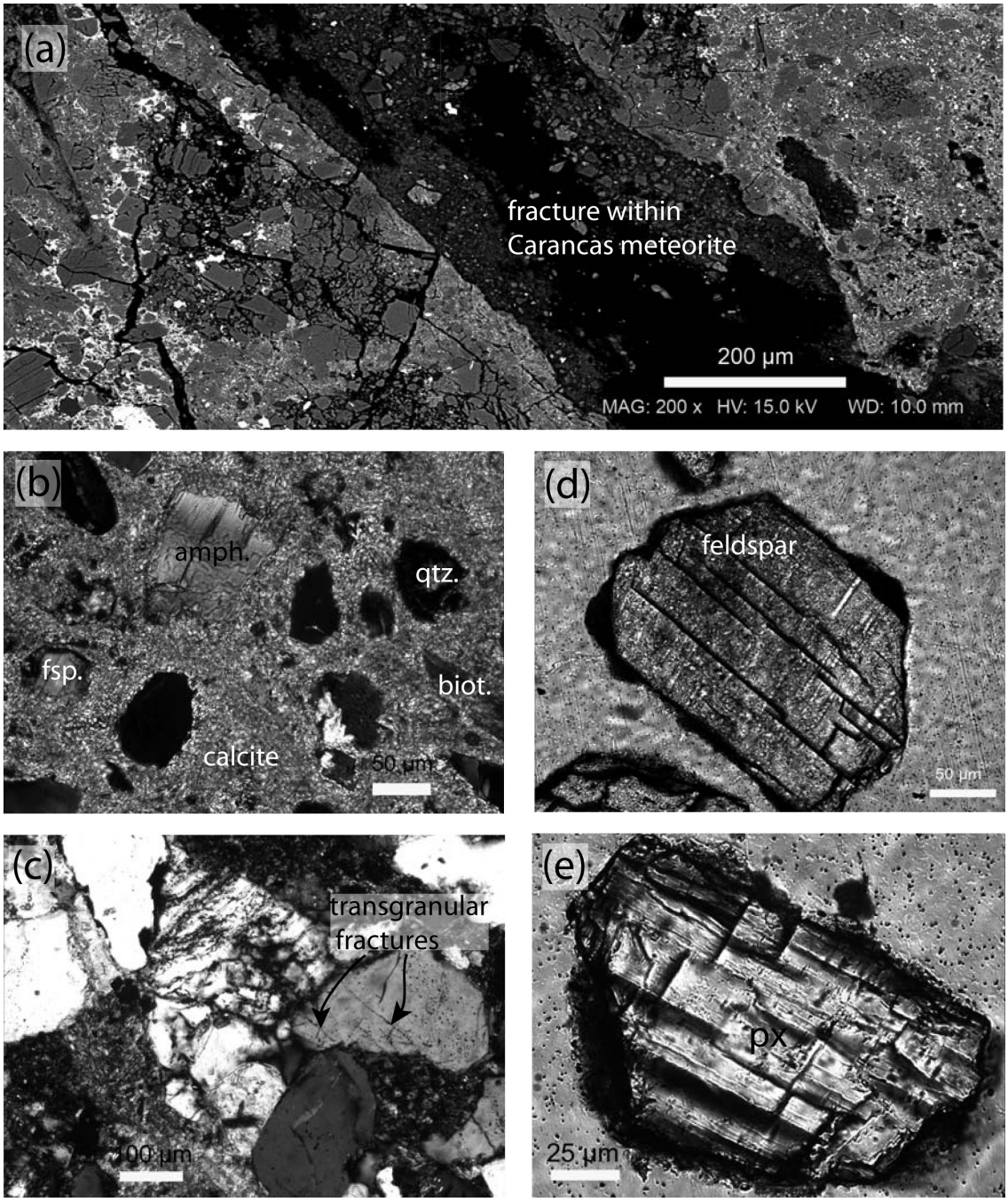

Fig. 5. a) Samples of the Carancas meteorite contain numerous fractures as well as polished and striated dark surfaces. The SEM-BSE image displays a fracture filled with comminuted olivine and pyroxene fragments. No signs of frictional melting due to shear heating could be observed. b) Fragment of excavated Puno-Group sand/siltstone consisting of quartz, feldspar, biotite, amphibole and opaque phases, and polymineralic rock fragments embedded in a matrix of calcite (crossed polarizers). c) Ejected quartz-feldspar rock fragment with transgranular fractures that could probably be related to the impact event (crossed polarizers). d and e) Orthoclase grains with {010} and {001} cleavage planes (linear polarizers). Note that no shock features could be found in any samples.

through the atmosphere we applied the atmospheric entry model (Artemieva and Shuvalov 2001; Bland and Artemieva 2006) that calculates the ablation mass rate and aerodynamic loading for meteoroid bodies and their fragments (if any). The following values are used in the model: a density of 3700 kg/m^3 (Consolmagno et al. 1998); an ablation coefficient of 0.004–0.008 s^2/km^2 (Ceplecha and ReVelle 2005); a drag coefficient of 0.5 (typical for a sphere) and 0.85 (typical for a blunt body); an entry velocity of 14 km/s (higher or lower velocity leads to obvious changes in dynamic pressure). Pre-atmospheric mass, and entry angle were varied to find a combination that resulted in a transient crater size which

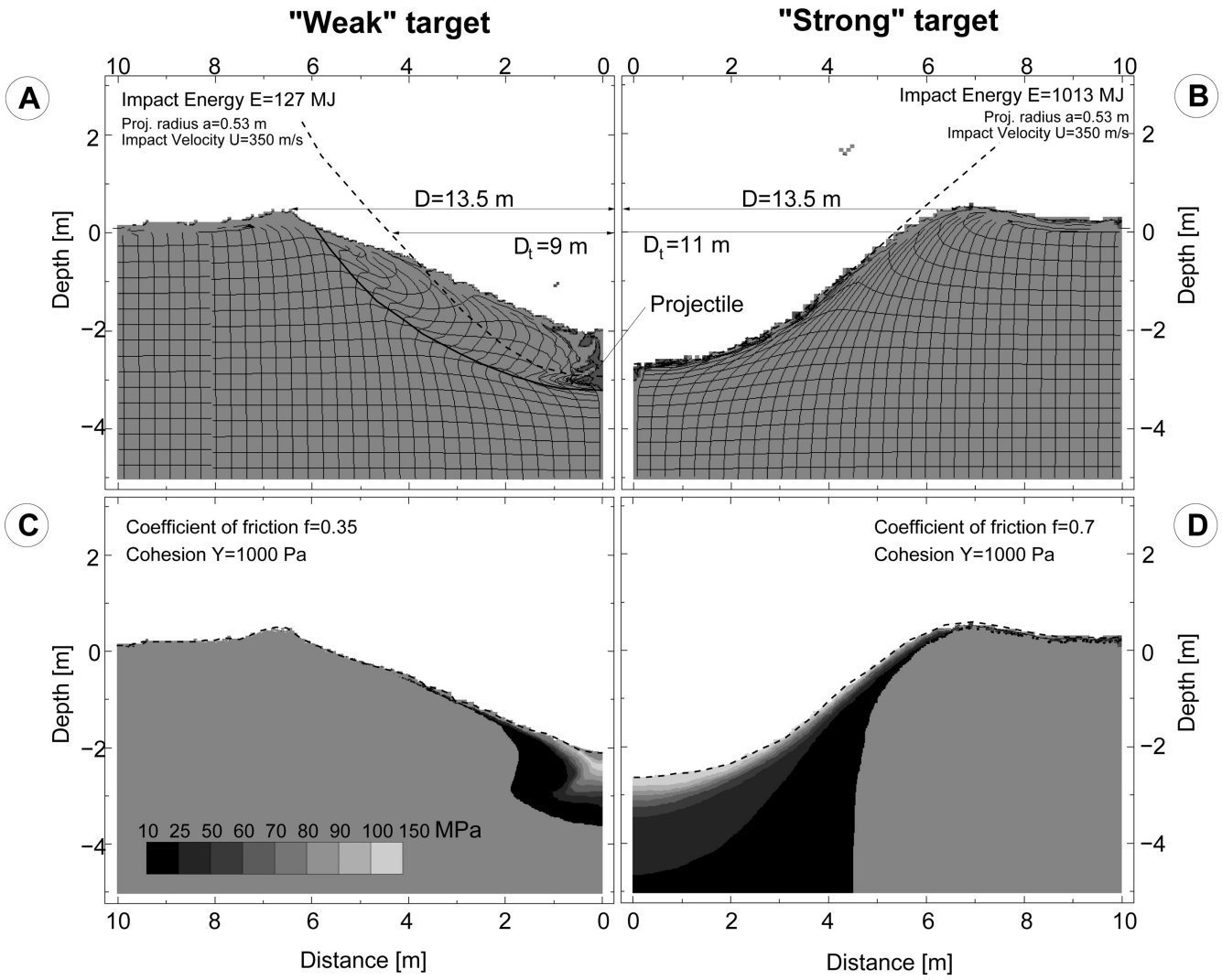

Fig. 6. Results of two-dimensional numerical modeling of crater formation carried out with the *iSALE* hydrocode (Wünnemann et al. 2006). A) Crater in a weak target. Due to slumping of the slope the crater is cone shaped and has a depth/diameter ratio of 0.18. Due to slumping a major fraction of the projectile is buried ~1 m beneath the crater floor. B) The crater with a strong target is bowl shaped and has a depth/diameter ratio of 0.23. Relics of the projectile are expected to cover the crater floor. C and D) Pressure distribution in the weak and strong target. The target volume exceeding stresses of 150 MPa is very low.

corresponds to the Carancas crater. Note that 2D modeling and scaling laws described in the previous section do not account for impact obliquity. We assume that the same scaling is applicable for an oblique impact, if the impact velocity is substituted by its vertical component as suggested by Chapman and McKinnon (1986). Numerical modeling of crater formation has shown that a transient crater diameter of 9 m for a "weak" rheology and 11 m for the "strong" target yield a final crater size of 13.5 m, measured from crest to crest.

The lines in Fig. 8 are constructed under the condition that impact velocity, angle, and mass are sufficient to produce a crater the size of Carancas. They show that in principle, for any pre-atmospheric angle combined with a cosmic velocity of 14 kms^{-1} a Carancas-like crater size can be obtained. The black line corresponds to the "weak" target, the grey line to the "strong" target. However, atmospheric trajectory and the aerodynamic loading to which the meteoroid is subjected to vary substantially. We distinguish two scenarios that grade into one another: (i) a steep (40–90° from the horizon) and (ii) an oblique to highly oblique (8–40°) pre-atmospheric entry angle.

1. For entry angles >40° (steep scenario), the meteoroid trajectory remains almost straight (the entry angle is equal to the impact angle) (Fig. 8b) and the impact velocity at the surface ranges between 500–600 ms^{-1} and 1000–1200 ms^{-1} for weak and strong target properties, respectively (Fig. 8c). The pre-entry masses required to produce Carancas-sized craters increase with increasing obliquity and range between 2000 (almost

Table 1. Mass and volume of material that experienced a certain pressure level upon impact, calculated for a weak and strong target. Note that shock pressures larger than 3 GPa occur only in a very small volume that is restricted to the projectile.

	Weak target				Strong target			
	Including projectile		Excluding projectile		Including projectile		Excluding projectile	
Pressure (GPa)	Mass (t)	Volume (m^3)	Mass (t)	Volume (m^3)	Mass (t)	Volume (m^3)	Mass (t)	Volume (m^3)
>0.05	3.64	1.54	2.13	1.08	12.26	5.22	7.37	3.74
>0.1	1.42	0.57	0.659	0.334	5.24	2.10	2.54	1.29
>0.5	0.093	0.033	0.024	0.012	0.338	0.120	0.088	0.047
>1	0.027	0.009	0.0032	0.0016	0.058	0.019	0.0064	0.0032
>2	0.007	0.002	0.0004	0.0002	0.015	0.0045	0.0008	0.0004

vertical, weak target) and 12000 kg (30°, strong target). Of great importance are the high aerodynamic stresses (12–18 MPa) that occur during atmospheric passage (Fig. 8d). These stresses are substantially higher than the strength of the majority of observed stony meteorites. Ceplecha et al. (1993) analyzed 80 bolides that were classified as ordinary or carbonaceous chondrites. They found that all fragmented bodies of relatively small size (2–2000 kg) were disrupted under apparent loading <1.2 MPa. Half of them were fragmented under loading <0.35 MPa. Moreover, these calculated stresses (12–18 MPa) are higher than the strengths of 11–12 MPa reported for two unusual events: Neuschwanstein (Spurný 2003) and EN171101 (Spurný and Porubčan 2002). If aerodynamic stresses exceed the strength of the meteoroid, it will be subjected to fragmentation. Figure 8d displays the stresses for an entry velocity of 14 kms^{-1}. For higher cosmic velocities aerodynamic loading increases further.

2. Oblique to highly oblique entry angles result in a substantial deceleration at the lower part of the trajectory down to free-fall velocity (Fig. 8c). Due to the strong deceleration, the impact angle becomes much steeper than the entry angle (Fig. 8b). For instance, at a highly oblique entry angle of 10°, an oblique impact of 50° to 70° (Fig. 8b) at a terminal velocity of 200–300 ms^{-1} (Fig. 8c) occurs on the ground (altitude 3800 m) and meets the conditions required to produce a Carancas-sized crater in a weak and a strong target, respectively. Most importantly, the maximum aerodynamic loading substantially decreases in comparison to steep entry angles and becomes less than 5 MPa for entry angles of 10° (Fig. 8c). Although this requires substantially higher pre-atmospheric masses (8–50 tons) (Fig. 8a), it provides realistic conditions to prevent a fragmentation of the stony meteoroid. Oblique entry angles explain the Carancas cratering event within our standard knowledge of meteorites, i.e., (i) the dynamic strength of the Carancas meteorite could be as low as 2–10 MPa, and is not necessarily anomalously high as suggested in Borovička and Spurný (2008) (therein 20–40 MPa is assumed) and (ii) there is no need for a special aerodynamic needle-like arrangement of the projectile to prevent fragment dispersion (Schultz et al. 2008).

To summarize, steep entry angles lead to aerodynamic stresses that exceed the common strength of stony meteorites and would cause substantial fragmentation. Under such conditions a meteorite strewn field, and not an isolated crater as in the case of the Carancas event is expected. To prevent fragmentation either abnormal strength of the meteoroid must be assumed (Borovička and Spurný 2008) or low aerodynamic stresses are required which in turn can be achieved if the cosmic velocity is low and if the entry angle is oblique to highly oblique. Under these circumstances the projectile substantially decelerates, thereby approaching terminal velocity and steepening its trajectory.

DISCUSSION

Pressure, Energy, and Crater Scaling

The main and consistent result of our combined approach of geological surveying, crater modeling, and modeling the atmospheric traverse is that the impact was not sufficient to cause a shock metamorphic overprint in the rocks. Shock pressures in the order of 1–2 GPa affect less than 20 dm^3 of the target plus projectile (Table 1). Considering the target alone this volume decreases to 1.6–3.2 dm^3. This cannot substantiate the findings of Harris et al. (2008) and Cardona et al. (2008).

By means of hydrocode modeling of crater formation we have demonstrated that the kinetic energy required to produce a Carancas-sized crater strongly depends on the target properties. Within a realistic range of strength properties for dry and wet soil (sand), we find kinetic impact energies approximately between 100–1000 MJ which is roughly in agreement with scaling laws for dry and water-saturated sand, but much less than previous estimates by Tancredi et al. (2008a, 2008b; 8,000–13,000 MJ) and Le Pichon et al. (2008; 20,000 MJ). Due to scaling laws (Equation 1; e.g., Holsapple and Housen 2007) such high energies can be only explained by assuming an extremely high cohesive strength for the target of more than 100 MPa, which is unrealistic for unconsolidated soil or sand having typically no or very little cohesive strength depending on wetting (Rajarama and

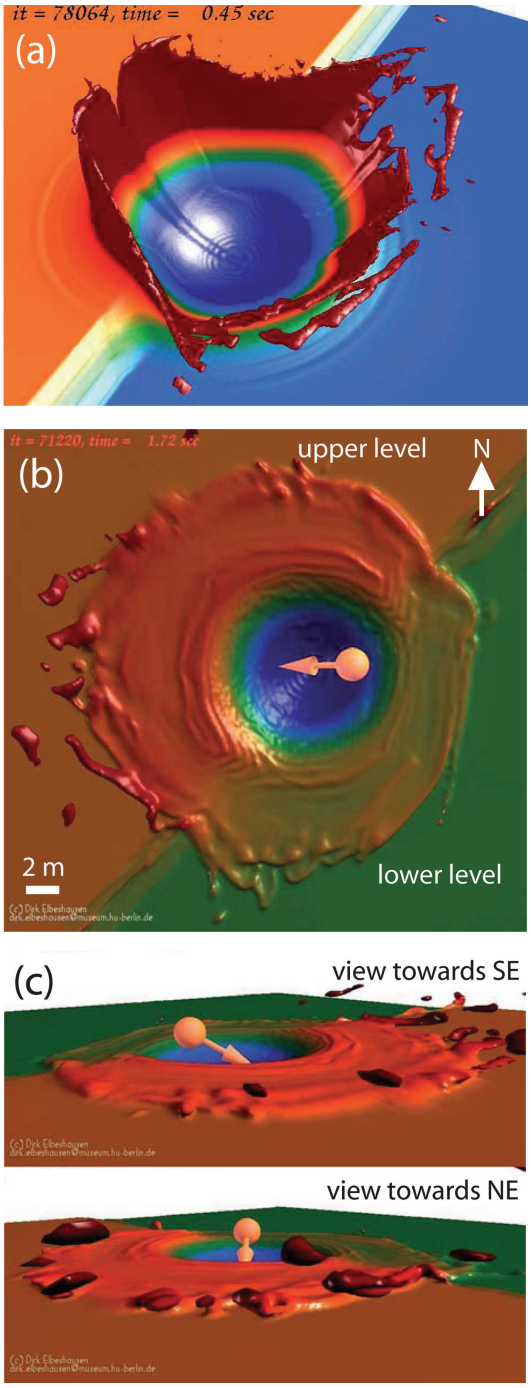

Fig. 7. Three-dimensional modeling using the same input parameters as in the 2D model but taking the topography of the target into account. The projectile hits a 1 m high slope of 30° inclination. a) Vertical impact: the slope has a strong effect on the kinematics of the excavation flow. Ejection angles are much steeper towards the higher target level than in the direction of the lower target level. The shape of the cavity deviates from circularity. b) 40° oblique impact from E, plan view. The final crater shape is circular and not affected by the slope. The extent of the ejecta blanket is reduced in uprange direction. Distribution and extent of the ejecta blanket correlates with the Carancas crater. c) Perspective view from the upper target level toward SE and NE.

Erbach 1999; 0–4 kPa). Scaling laws have to be used with caution as the results strongly depend on the mechanical properties of the target and scaling parameters are only available for some very specific types of materials (e.g., dry and water-saturated sand). Hydrocode modeling provides more accurate estimates of the energy since material properties such as friction and strength can be varied independently within realistic estimates. Moreover, they provide additional information on crater morphology that can be compared with field observations.

According to scaling laws (Equation 1; e.g., Holsapple and Housen 2007), the impact energy for the Carancas event could not have been any higher than 3000 MJ, assuming the highest estimate for a possible impact velocity of U = 6 kms^{-1} (Harris et al. 2008) and relatively strong target properties (dry sand). However, for the numerical models of crater formation we achieved the best agreement with morphological and morphometric observations for an approximate impact energy of 1000 MJ, an impact velocity of 600 ms^{-1}, a cohesive strength of 1 kPa, and a coefficient of friction $f = 0.7$.

Impact Velocity

Schultz et al. (2008) and others suggested that the Carancas event was caused by a relatively high-velocity impact on the order of 1 to 6 kms^{-1}. High speeds could be sustained by reshaping of the meteoroid into an aerodynamic train of fragments. They argued that the so-called "pancake model" (Chyba et al. 1993), which assumes a flattening of the projectile at constant mass during atmospheric traverse, is not applicable to the Carancas meteoroid fall. In fact, experiments by Sugita and Schultz (1995) showed that under certain conditions, e.g., high atmospheric pressure, fragments do not disperse but are collimated within the shock wave behind the leading (usually the largest) body. This scenario was confirmed by numerical simulations (Artemieva and Shuvalov 1996). The model also indicated that the leading body in supersonic flow does not "feel" the train of fragments in its wake and is subjected to the same severe conditions (i.e., dynamic loading and drag) as an isolated fragment. At the same time fragments within the wake are in a hydrodynamic shadow, i.e., dynamic loading is extremely low and substantial increase of energy release in the atmosphere after the disruption does not occur (no light flash, no peaks in infrasound or seismic signals, which are usually associated with the disruption). However, if another fragmentation occurs and leading fragments, which are subjected to the full aerodynamic stress, become smaller than those in the wake, the swarm is re-organized so that the largest fragment is at the leading position (which can be subjected to the next fragmentation and so on). Our estimates for this scenario (using standard strength for stony bodies) shows that (i) it would require a much larger mass in the upper atmosphere, and (ii) it may result in final velocities that are substantially

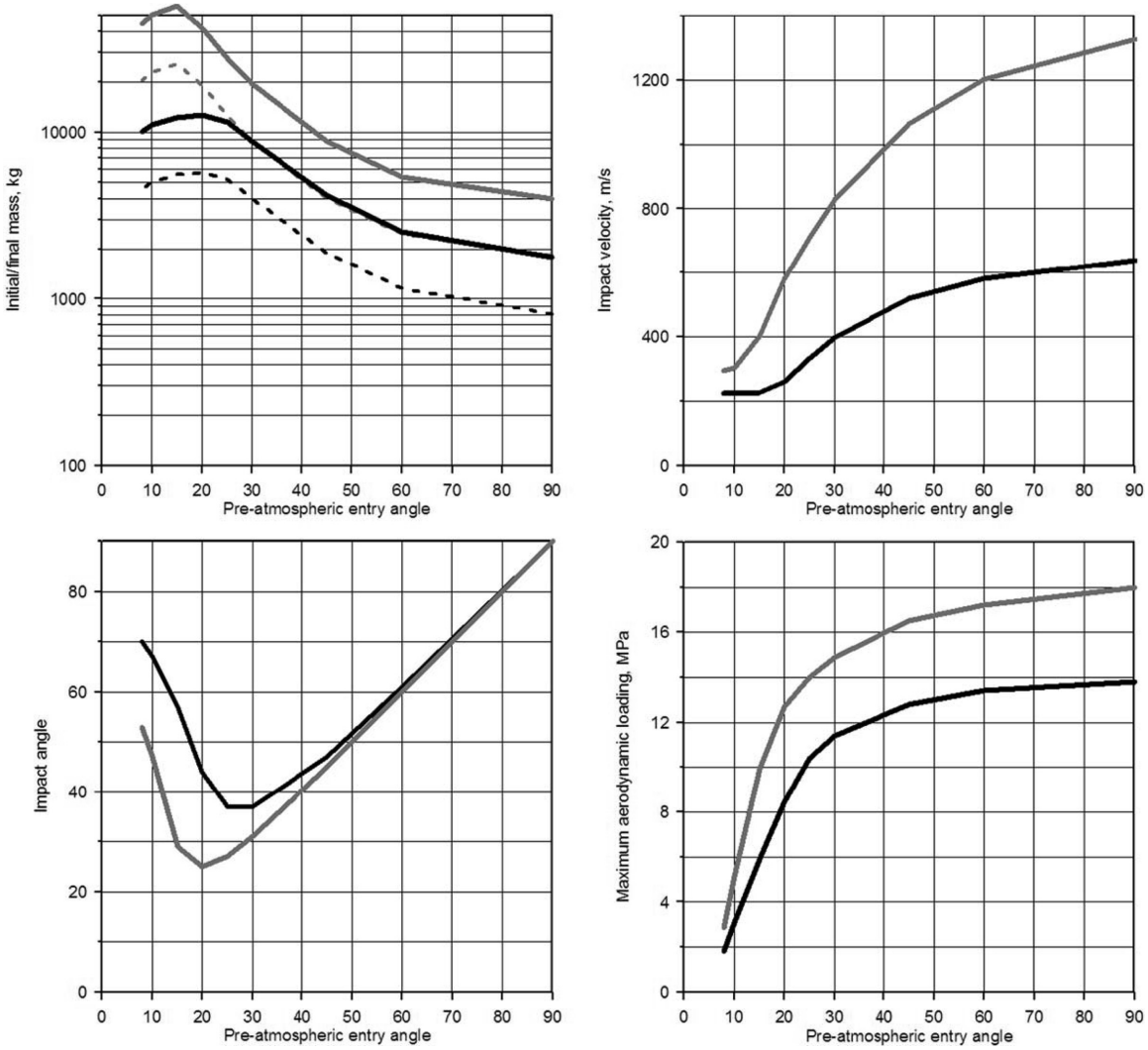

Fig. 8. Results from the model of atmospheric entry. The entry velocity is kept constant at 14 kms^{-1}. The gray and black lines represent conditions that lead to Carancas-sized craters assuming a strong and weak target rheology, respectively. A) Pre-atmospheric entry angle versus initial and final meteoroid mass (stippled lines). Larger masses are required to obtain Carancas-sized craters if the pre-atmospheric entry angle is shallow. B) Pre-atmospheric entry angle versus impact velocity. Terminal velocity is reached for shallow entry angles. C) Pre-atmospheric entry angle versus impact angle. The impact angle is steeper than the pre-atmospheric entry angle for entry angles of less than 50° and 30° for weak and strong targets, respectively. D) Pre-atmospheric entry angle versus aerodynamic stresses. A remarkable drop in dynamic loading occurs for entry angles of 30° and less.

below 1 kms^{-1}. Our modeling shows that a specific arrangement of meteoroid fragments is not required to prevent fragmentation if an initial shallow entry angle and a low cosmic velocity are assumed.

Meteoroid Strength

The compressive strength of centimeter-sized meteorites measured in the laboratory is usually in the range of a few hundred MPa, while the tensile strength is an order of magnitude lower (see review by Svetsov et al. 1995). In contrast to this, astronomical observations (Ceplecha et al. 1993) show that meteoroid disruptions commonly occur at altitudes where dynamic loading is in the order of about 1 MPa, i.e., several orders of magnitude lower than static loading tests (Ceplecha et al. 1993). Standard size scaling in rock mechanics, known as Weibull (1951) statistics, is usually applied to explain this discrepancy. The size dependency of strength works for any rocks (e.g., Adey and Pusch 1999), including meteorites. However, it should be treated statistically, i.e., it yields an average value from which the strength of individual "rocks" can differ in certain limits. Unfortunately, statistics on the strength of large, meter-sized meteoroids are still restricted to a few tens of observations (Popova and Nemtchinov 2002), involving meteoroids with various masses and compositions, and hence, it does not allow the range of deviation from the average value to be defined accurately. However, 20–40 MPa values for the Carancas

meteoroid, as suggested by Borovička and Spurný (2008), by far exceed previous observations (Ceplecha et al. 1993). The model presented above demands values of half the size at 18 MPa (Fig. 8d) even for the scenario of a sub-vertical impact into rocks with high friction. Nonetheless, even the value of 18 MPa is almost two times higher than the extreme values of 11–12 MPa observed for the Neuschwanstein meteorite (Spurný et al. 2003) and EN171101 fireball (Spurný and Porubčan 2002). It is worth mentioning that both of these meteoroids have an order of magnitude smaller mass than Carancas (i.e., the Neuschwanstein's entry mass was 300 kg, and the mass of the EN171101 largest fragment was 450 kg) and according to Weibull's law (Weibull 1951) should have higher strength than the Carancas meteoroid. As all meteorites underwent collisional evolution in the Main Asteroid Belt, the monolithic block proposed by Borovička and Spurný (2008) is highly questionable, although it cannot be dismissed totally.

Our preferred scenario of a shallow entry angle is in conflict with interpretations of infrasound and seismic data (Brown et al. 2008; Le Pichon et al. 2008). These data suggest atmospheric entry angles of 50–63° at 12 kms^{-1}, which, according to Fig. 8d, require a meteoroid of very high strength. The recorded infrasound signals were relatively weak and were interpreted in different ways by different groups. Brown et al. (2008) stated that the observed signal was produced by the impact itself, while Le Pichon et al. (2008) preferred to relate the same signal with atmospheric disruptions. The infrasound propagation is significantly affected by the vertical and horizontal wind structure where wind-induced refraction can trap or disperse sound energy (Le Pichon et al. 2008). This is particularly relevant for the station at 1617 km distance. The interpretation of the infrasound signal is based on the assumption of a straight trajectory, which may not be true. Furthermore they did not explain the discrepancy of one order of magnitude between measured and modeled overpressure signal. Thus the inferred data must be taken with caution, in particular as no error bars were given for their results.

Probability of Carancas-Like Events

Impact-induced damage of the ground and the environment from the formation of the Carancas crater and by the impact of the proximal and distal ejecta is restricted to an area of about 0.2 km^2. If the impact had occurred in a populated area instead of the remote area of the Altiplano, the event might have caused a severe number of human casualties. Considering the mean world population density (50 inhabitants per square-kilometer), statistically, ten people could have been affected. Thus, the risk of Carancas-like events must be taken into account in future impact probability assessment studies. As detailed before, conditions that increase the survivability of small bodies during their traverse through the atmosphere include low cosmic velocities, oblique entry angles, and, of course, the composition of the body. Iron meteoroids transfer three orders of magnitude more energy per unit area than stony meteoroids over the mass range of 10^3–10^7 kg (Bland and Artemieva 2006). The high altitude of the Altiplano (3824 m) did not affect survivability of the stony meteoroid as the maximum aerodynamic stresses occurred at a height of 20–45 km. To determine the impact probability for Carancas-like scenarios the number of meter-sized projectiles approaching the Earth's atmosphere needs to be known. The number of Earth approaching asteroids with roughly ten tons of entry mass is in the order of ten events per year (Bland and Artemieva 2003, 2006). Combining this with the probability of impacts occurring at shallow angles (less than 15°), which is 6.7% (Pierazzo and Melosh 2000) and the fraction of Earth crossing asteroids with a cosmic velocity below 13.8 kms^{-1} which is ~25% (Steel 1998), the likelihood of a Carancas-like impact that is capable of penetrating the atmosphere without disruption is about one event every ten years. In the wake of the centenary of the Tunguska event, previously unconsidered impacts like Carancas show that the impact risk on Earth has been underestimated.

CONCLUSIONS

Carancas is currently the youngest and smallest known impact crater on Earth, and together with the Sterlitamak cratering event in 1990 (Petaev et al. 1991; Ivanov and Petaev 1992), the first that was observed by witnesses. The results of our geologic surveying, subsequent microscopic investigations, and modeling of crater formation and atmospheric passage have common implications: the most important is that the impact was not sufficient to cause any significant shock metamorphic overprint in the rocks. Crater modeling in two and three dimensions revealed that the impact energies range between approximately 100–1000 MJ (0.024–0.24 t TNT), depending on the strength properties of the target. To keep the aerodynamic stresses during the passage through the atmosphere low (<10 MPa) and thus to prevent fragmentation of stony meteoroids with standard strength properties, cosmic velocities must be low (12–14 kms^{-1}) and entry angles must be shallow (<20°). This scenario would result in a strong meteoroid deceleration, a deflection of the trajectory to a steeper impact angle (40–60°), and an impact velocity of 350–600 ms^{-1}. While our preferred scenario is in agreement with field surveying it is in conflict with a steep meteoroid entry (50–63°; Le Pichon et al 2008; Brown et al. 2000) inferred from the analysis of infrasound and seismic signals. Such a scenario would require stony meteorites of extreme dynamic strength of 20–40 MPa.

Acknowledgments–We are grateful to the Museum für Naturkunde for providing travel funding. NAA acknowledges

the support by the German Research Foundation (DFG). Local assistance in Peru is also greatly acknowledged. We thank Boris Ivanov and an anonoumous reviewer for thoughtful reviews.

Editorial Handling—Dr. Gordon Osinski

REFERENCES

Adey R. A. and Pusch R. 1999. Scale dependency in rock strength. *Engineering Geology* 53:25l–258.

Allen R. T. 1967. Equations of state of rocks and minerals. Interim report to DASA under contract DA 49–146-XZ-462. General Dynamics Report #GA MD-7834.

Artemieva N. A. and Shuvalov V. V. 1996. Interaction of shock waves during the passage of a disrupted meteoroid through the atmosphere. *Shock Waves* 5:359–367.

Artemieva N. A. and Shuvalov V. V. 2001. Motion of a fragmented meteoroid through planetary atmosphere. *Journal of Geophysical Research* 106 E2:3297–3309.

Baratoux D. and Melosh H. J. 2003. The formation of shatter cones by shock wave interference during impacting. *Earth and Planetary Science Letters* 216:43–54.

Benz W., Cameron A. G. W., and Melosh H. J. 1989. The origin of the Moon and the single impact hypothesis, III. *Icarus* 81:113–131.

Bland P. and Artemieva N. A. 2003. Efficient disruption of small asteroids by Earth's atmosphere. *Nature* 424:288–291.

Bland P. and Artemieva N. A. 2006. The rate of small impacts on Earth. *Meteoritics & Planetary Science* 41:607–631.

Borovička J. and Spurný P. 2008. The Carancas meteorite impact—Encounter with a monolithic meteoroid. *Astronomy and Astrophysics* 485:L1–L4.

Brown P., Spalding R. E., ReVelle D. O., Tagliaferri E., and Worden S. P. 2002. The flux of small near-Earth objects colliding with the Earth. *Nature* 420:294–296.

Brown P., ReVelle D. O., Silber E. A., Edwards W. N., Arrowsmith S., Jackson L. E., Tancredi G., and Eaton D. 2008. Analysis of a crater-forming meteorite impact in Peru. *Journal of Geophysical Research* 113:E09007, doi:10.1029/2008JE003105.

Cardona M. R., Núñez del Prado H., Machare J., Macedo L., Chirif H., Pari W., and Ramirez-Mendoza D. 2008. Shock metamorphic features in Carancas crater, Peru (abstract). International Geological Congress Oslo 2008.

Ceplecha Z., Spurný P., Borovička J., and Kecliková J. 1993. Atmospheric fragmentation of meteoroids. *Astronomy & Astrophysics* 279:615–626.

Ceplecha Z. and ReVelle D. O. 2005. Fragmentation model of meteoroid motion, mass loss, and radiation in the atmosphere. *Meteoritics & Planetary Science* 40:35–54.

Chapman C. R. and McKinnon W. B. 1986. Cratering of planetary satellites. In: *Satellites,* edited by Burns J. A. and Matthews M. S. Tucson: The University of Arizona Press. pp. 492–580.

Chyba C. F., Thomas P. J., and Zahnle K. J. 1993. The 1908 Tunguska explosion: Atmospheric disruption of a stony asteroid. *Nature* 361:40–44.

Connolly H. C., Smith C., Benedix G., Folco L., Righter K., Zipfel J., Yamaguchi A., and Chennaoui Aoudjehane H. 2007. The Meteoritical Bulletin, No. 93, 2008 March. *Meteoritics & Planetary Science* 43:571–632.

Consolmagno G. J., Britt D. T., and Stoll C. P. 1998. The porosity of ordinary chondrites: Models and interpretations. *Meteoritics & Planetary Science* 33:1221–1229.

Elbeshausen D., Wünnemann K., and Collins G. S. 2009. Scaling of oblique impacts in frictional targets: Implications for crater size and formation mechanisms. *Icarus*. In press.

Harris R. S., Schultz P. H., Tancredi G., and Ishitsuka J. 2008. Preliminary petrologic analysis of impact deformation in the Carancas (Peru) cratering event. 39th Lunar and Planetary Science Conference. Abstract #2446.

Holsapple K. A. 1993. The scaling of impact processes in planetary science. *Annual Review of Earth and Planetary Sciences* 21:333–373.

Holsapple K. A. and Housen K. R. 2007. A crater and its ejecta: An interpretation of Deep Impact. *Icarus* 187:345–356.

Ivanov B. A. and Petaev M. I. 1992. Mass and impact velocity of the meteorite formed the Sterlitamak crater in 1990 (abstract). 23rd Lunar and Planetary Science Conference. pp. 573–574.

Kenkmann T., Artemieva N. A., and Poelchau M. H. 2008a. The Carancas event on September 15, 2007: Meteorite fall, impact conditions and crater characteristics. 39th Lunar and Planetary Science Conference. Abstract #1094.

Kenkmann T., Artemieva N. A., Wünnemann K., Poelchau M. H., Elbeshausen D., and Núñez del Prado H. 2008b. The remarkable meteorite impact event on September 15, 2007, Carancas, Peru: What did we learn? *Large Meteorite Impacts and Planetary Evolution IV,* Parys, South Africa.

Le Pichon A., Antier K., Cansi Y., Hernandez B., Minaya E., Burgoa B., Drob D., Evers L. G., and Vaubaillon J. 2008. Evidence of a meteoritic origin of the September 15th, 2007 Carancas crater. *Meteoritics & Planetary Science* 43:1797–1809.

Macedo L. and Macharé J. 2007. The Carancas meteorite fall, 15 September 2007. Official INGEMMET initial report. http://www.ingemmet.gob.pe/.

Miura Y. 2007. Multiple explosions durino cratering at Carancas meteorite hit in Peru. 39th Lunar and Planetary Science Conference. Abstract #2027.

Morrison D. 2002. Target Earth. *Astronomy* 30:46–51.

Núñez del Prado H., Macharé J., Macedo L., Chirif H., Pari W., Ramirez-Cardona M., Aranda A., Greenwood R. C., Franchi I. A., Canepa C., Bernhardt H.-J., and Plascencia L. 2008. The meteorite fall in Carancas, Lake Titicaca region, southern Peru: First results. 39th Lunar and Planetary Science Conference. Abstract #2555.

O'Keefe J. D. and Ahrens T. J. 1993. Planetary cratering mechanics. *Journal of Geophysical Research* 98, E9:17011–17028.

Ostertag R. 1983. Shock experiments on feldspar crystals. *Journal of Geophysical Research* 88:B364–B376.

Petaev M. I., Kisarev Y. L., Mustafin S. A., Shakurov R. K., Pavlov A. V., and Ivanov B. A. 1991. Meteorite Sterlitamak-A new crater forming fall (abstract). 22nd Lunar and Planetary Science Conference. pp. 1059–1060.

Petrovic J. J. 2001. Mechanical properties of meteorites and their constituents. *Journal of Material Science* 36:1579–1583.

Pierazzo E. and Melosh H. J. 2000. Understanding oblique impacts from experiments, observations, and modelling. *Annual Review of Earth and Planetary Sciences* 28:141–167.

Popova O. P. and Nemchinov I. V. 2002. Strength of large meteoroids entering Earth atmosphere. In *Proceedings of Asteroids, Comets, Meteors—ACM 2002*, edited by Warmbein B. European Space Agency Special Paper 500. pp. 281–284.

Rajarama G. and Erbach D. C. 1999. Effect of wetting and drying on soil physical properties. *Journal of Terramechanics* 36:39–49.

Rosales D., Vidal E., Ishitsuka J., and Benavente S. 2008. Geomagnetic study of Carancas meteorite and its crater. 39th Lunar and Planetary Science Conference. Abstract #1744.

Schmidt R. M. and Housen K. R. 1987. Some recent advances in the scaling of impact and explosion cratering. *International Journal of Impact Engineering* 5:543–560.

Schultz P. H., Harris R. S., Tancredi G., and Ishitsuka J. 2008. Implications of the Carancas meteorite impact. 39th Lunar and Planetary Science Conference. Abstract #2409.

Spurný P. and Porubčan V. 2002. in *Proceedings of Asteroids, Comets, Meteors—ACM 2002*, edited by Warmbein. B. European Space Agency Special Paper 500. pp. 281–284.

Spurný P., Oberst J., and Heinlein D. 2003. Photographic observations of the Neuschwanstein, a second meteorite from the orbit of the Příbram chondrite. *Nature* 423:151–153.

Steel D. 1998. Distributions and moments of asteroid and comet impact speeds upon the Earth and Mars. *Planetary and Space Science* 46:473–478.

Stöffler D. and Langenhorst F. 1994. Shock metamorphism of quartz in nature and experiment: I. Basic observation and theory. *Meteoritics* 29:155–181.

Sugita S. and Schultz P. H. 1995. Dynamical evolution of vapor clouds by oblique impacts on Venus (abstract). 26th Lunar and Planetary Science Conference. pp. 1369–1370.

Svetsov V. V., Nemtchinov I. V., and Teterev A. V. 1995. Disintegration of large meteoroids in Earth's atmosphere: Theoretical models. *Icarus* 116:131–153.

Tancredi G., Ishitsuka J., Rosales D., Vidal E., Dalmau A., Pavel D., Benavente S., Mirando P., Pereira G., Vallejos V., Varela M. E., Brandstätter F., Schultz P., Harris R. S., and Sanchez L. 2008a. What do we know about the "Carancas-Desaguadero" fireball, meteorite and impact crater? Lunar and Planetary Science Conference 39: abstract #1216.

Tancredi G., Ishitsuka J., Schultz P. H., Harris R. S., Brown P., Revelle D., Antier K., LePichon A., Rosales D., Vidal E., Pavel D., Dalmau A., Benavente S., Mirando P., Pereira G., Varela M. E., and Sanchez L. 2008b. The Carancas crater and meteorite fall: the first recorded impact on Earth. Asteroids, Comets, Meteors Conference. Abstract #8260.

Thompson S. L. and Lauson H. S. 1972. Improvements in the Chart D radiation-hydrodynamic code 3: Revised analytic equation of state: Report SC-RR-71 0714, Albuquerque, New Mexico, Sandia Laboratories. 119 p.

Tillotson J. H. 1962. Metallic Equations of State for Hypervelocity Impact. General Atomic Division of General Dynamics Report GA-3216, San Diego, CA.

Trigo-Rodríguez J. M., Borovička J., Spurný P., Ortiz J. L., Docobo J. A., Castro-Tirado A. J., and Llorca J. 2006. The Villalbeto de la Pena meteorite fall: II. Determination of atmospheric trajectory and orbit. The rate of small impacts on Earth. *Meteoritics & Planetary Science* 41:505–517.

Tsvetkov V. I. 1983. Connection of fragmentation and scattering of the Sikhote-Alin meteorite shower with meteorite structure. *Solar System Research* (Engl. Transl.) 17:122–126.

Weibull W. 1951. A statistical distribution function of wide applicability. *Journal of Applied Mechanics* 18:140–147.

Wünnemann K., Collins G. S., and Melosh H. J. 2006. A strain-based porosity model for use in hydrocode simulations of impacts and implications for transient crater growth in porous targets. *Icarus* 180:514–527.